


ORIGINAL ARTICLE

PRMT3 regulates the progression of invasive micropapillary carcinoma of the breast

Renyong Zhi^{1,2,3,4,5}  | Kailiang Wu^{1,2,3,4,5} | Jingyue Zhang^{1,2,3,4,5} | Hanjiao Liu^{1,2,3,4,5} | Chen Niu^{1,2,3,4,5} | Shuai Li^{1,2,3,4,5} | Li Fu^{1,2,3,4,5}

¹Department of Breast Cancer Pathology and Research Laboratory, Tianjin Medical University Cancer Institute and Hospital, Tianjin, China

²National Clinical Research Center of Cancer, Tianjin, China

³Key Laboratory of Cancer Prevention and Therapy, Tianjin, China

⁴Tianjin's Clinical Research Center for Cancer, Tianjin, China

⁵Key Laboratory of Breast Cancer Prevention and Therapy, Tianjin Medical University, Ministry of Education, Tianjin, China

Correspondence

Li Fu and Shuai Li, Department of Breast Cancer Pathology and Research Laboratory, Tianjin Medical University Cancer Institute and Hospital, Tianjin, 300060, China.
Email: fuli@tmu.edu.cn, shuaili@tmu.edu.cn

Funding information

National Natural Science Foundation of China, Grant/Award Number: 31870860, 81872164 and 82173344

Abstract

Invasive micropapillary carcinoma (IMPC) is a special histopathological subtype of breast cancer. Clinically, IMPC exhibits a higher incidence of lymphovascular invasion and lymph node metastasis compared with that of invasive ductal carcinoma (IDC), the most common type. However, the metabolic characteristics and related mechanisms underlying malignant IMPC biological behaviors are unknown. We performed large-scale targeted metabolomics analysis on resected tumors obtained from chemotherapy-naïve IMPC ($n = 25$) and IDC ($n = 26$) patients to investigate metabolic alterations, and we integrated mass spectrometry analysis, RNA sequencing, and ChIP-sequencing data to elucidate the potential molecular mechanisms. The metabolomics revealed distinct metabolic profiles between IMPC and IDC. For IMPC patients, the metabolomic profile was characterized by significantly high levels of arginine methylation marks, and protein arginine methyltransferase 3 (PRMT3) was identified as a critical regulator that catalyzed the formation of these arginine methylation marks. Notably, overexpression of PRMT3 was an independent risk factor for poor IMPC prognosis. Furthermore, we demonstrated that PRMT3 was a key regulator of breast cancer cell proliferation and metastasis both in vitro and in vivo, and treatment with a preclinical PRMT3 inhibitor decreased the xenograft tumorigenic capacity. Mechanistically, PRMT3 regulated the endoplasmic reticulum (ER) stress signaling pathway by facilitating histone H4 arginine 3 asymmetric dimethylation (H4R3me2a), which may endow breast cancer cells with great proliferative and metastatic capacity. Our findings highlight PRMT3 importance in regulating the malignant biological behavior of IMPC and suggest that small-molecule inhibitors of PRMT3 activity might be promising breast cancer treatments.

Abbreviations: ADMA, Asymmetric N^G, N^G -dimethylarginine; ASL, Arginine succinate lyase; DTCs, Disseminated tumor cells; EMA/MUC1, Epithelial membrane antigen; ER, Endoplasmic reticulum; EZH2, Enhancer of zeste homolog 2; FOXP1, Forkhead box protein P1; GSSG, Glutathione disulfide; H3K4me3, Histone H3 lysine 4 trimethylation; H3R2me2s, Histone H3 arginine 2 symmetrical dimethylation; H4R3me2a, Histone H4 arginine 3 asymmetric dimethylation; IDC, Invasive ductal carcinoma; IMPC, Invasive micropapillary carcinoma; MLL, Mixed-lineage leukemia; MMA, N^G -monomethylarginine; NOS, Nitric oxide synthase; Pol II, RNA polymerase II; PRMT3, Protein arginine methyltransferase 3; SDMA, Symmetric N^G, N^G -dimethylarginine; SET1, SET domain-containing protein 1, histone lysine methyltransferase; TES, Transcription termination site; TSS, Transcription start site; UPR, Unfolded protein response.

Renyong Zhi and Kailiang Wu authors contributed equally to this work.

This is an open access article under the terms of the [Creative Commons Attribution-NonCommercial-NoDerivs](https://creativecommons.org/licenses/by-nc-nd/4.0/) License, which permits use and distribution in any medium, provided the original work is properly cited, the use is non-commercial and no modifications or adaptations are made.

© 2023 The Authors. *Cancer Science* published by John Wiley & Sons Australia, Ltd on behalf of Japanese Cancer Association.

KEYWORDS

arginine methylation, breast cancer, metabolomics, metastasis, proliferation, protein arginine methyltransferases

1 | INTRODUCTION

Breast cancer is the most commonly diagnosed cancer in women, and cancer cell metastasis is the main cause of death.¹ IMPC is a special histopathological subtype of breast cancer that was first reported in 1993^{2,3} and is characterized by micropapillary or morula-like clusters of IMPC cells without fibrovascular cores surrounded by empty stromal spaces.⁴ Recently, IMPC has been identified in multiple organs, including the lung,⁵ colon,⁶ pancreas,⁷ and bladder.⁸ Clinically, IMPC of the breast leads to a higher incidence of lymphovascular invasion and lymph nodal metastasis and a worse prognosis than the IDC.⁹⁻¹¹ Furthermore, the micropapillary pattern of IMPC is retained not only in primary tumors but also in lymphovascular and lymph node metastatic foci.¹¹⁻¹³ Thus, the unique “clustered metastasis of IMPC tumor cells” renders IMPC a good model for studying biological behaviors in aggressive malignancy.¹⁴⁻¹⁶ Recent studies have reported genomic and spatial transcriptomic features of IMPC and suggested that its extensive heterogeneity is associated with metabolic reprogramming.^{15,16} However, deep insight into the metabolic characteristics and identification of metastasis-associated biomarkers remains elusive.

Metabolic reprogramming, a hallmark of cancer, is recognized as a driving force for cancer initiation and progression.¹⁷ Metabolomics is the global analysis of small-molecule metabolites that helps to identify novel biomarkers for cancer diagnostics, prognostics, or therapeutics.^{18,19} In a recent study, large-scale targeted metabolomics analysis of invasive lung adenocarcinoma and preinvasive lesions exhibited that dysregulated bile acid metabolism promoted cancer cell migration, suggesting an opportunity for potential targetable therapeutics.²⁰ Arginine methylation, as a posttranslational modification of proteins, has been increasingly shown to be associated with cancer progression.^{21,22} Moreover, protein arginine methyltransferases (PRMTs), which are the writers of arginine methylation, have been recently reported to be involved in dysregulated metabolism during tumorigenesis.^{23,24} PRMTs are classified into three types based on the methyl group they deposit: Type I enzymes (PRMT1, 2, 3, 4, 6, and 8) catalyze the formation of MMA and ADMA, type II enzymes (PRMT5 and 9) catalyze the formation of MMA and SDMA, and the type III enzyme (PRMT7) catalyzes the formation of MMA.²² Notably, a recent discovery suggested that PRMTs are overexpressed in solid and hematologic cancers, which are correlated with poor patient prognosis.^{25,26} However, an in-depth mechanistic investigation into the tumor and substrate specificities of PRMTs is needed.

In this study, the metabolomic profile of IMPC was evaluated and compared with that of IDC, and the results revealed aberrant arginine methylation in IMPC. PRMT3 was overexpressed in IMPC, which was associated with malignant progression and poor

prognosis. Using systematic *in vitro* methods to investigate the contribution of PRMT3 to breast cancer cell function, we demonstrated that PRMT3 interacted with histone H4 and enhanced the levels of H4R3me2a, which mediated the ER stress-related gene expression. Our findings are clinically significant, as genetic knockdown or a specific inhibitor of PRMT3 substantially decreased the growth of cancer cells in xenograft mouse models. This evidence sheds light on a novel pathway and potential therapeutic target in breast cancer.

2 | MATERIALS AND METHODS

2.1 | Collection of clinical samples

Patient tissue specimens were obtained from the Cancer Hospital of Tianjin Medical University between 2016 and 2017; these samples included those obtained from 26 patients with IDC and 25 patients with IMPC. None of the patients had received anti-tumor treatment before the operation, and all patients signed an informed consent agreement (Figure S1A). All tissues were cut into two samples based on the maximum diameter of the tumor, and one tissue was fixed after pathological sampling. After dehydration, embedding, and serial sectioning, the fixed tissue was exposed to H&E staining and EMA/MUC1 immunohistochemistry (IHC) staining (1:1000, ab109185; Abcam), which was performed to diagnose the samples. The independent diagnosis of two senior pathologists following the WHO classification criteria was the basis for determining whether a sample was included in the IDC group or the IMPC group. The unfixed tumor sample was cut into 5×5×5 mm cubes, transferred to liquid nitrogen, and stored at -80°C until metabolite extraction. The clinicopathological information for all the samples is shown in Table S1.

2.2 | Metabolite extraction and targeted metabolomics analysis

Metabolite extraction and targeted metabolomics analysis were performed as described previously.²⁰ Briefly, all samples from 51 patients were divided randomly into one analytical batch. Each sample was weighed precisely and homogenized in cold 80% methanol solution (50 mg tissue/mL), then vortexed, and centrifuged at 4°C at 15,000 g for 15 min. The supernatant was collected and dried under a high-speed vacuum concentrator. The dried metabolite particles were re-dissolved in formic acid in analytical grade water, mixed, and then centrifuged to remove fragments. Next, the supernatant was measured for targeted metabolite profiling using a liquid chromatography-mass spectrometry/mass spectrometry (LC-MS/

MS) approach. Chromatographic separation was performed using an Acquity UPLC I-Class system (Waters Corp.), coupled with a Xevo TQ-XS mass spectrometer (Waters Corp.). We collected and classified the metabolites based on the Human Metabolome Database (HMDB) (<http://hmdb.ca>). Raw data preprocessing and normalization were performed as described previously.^{20,27} The further analyses of metabolic differences between IMPC and IDC, including principal component analysis (PCA) and Kyoto Encyclopedia of Genes and Genomes (KEGG) pathway enrichment analysis, were performed using the “prcomp” and “clusterProfiler” functions in the R package, respectively.

2.3 | Real-time qPCR

Analysis of mRNA expression was performed as described previously.²⁸ Total RNA was isolated using TRIzol reagent (Invitrogen) and reverse transcribed using a High Capacity cDNA Reverse Transcription Kit with random primers (Applied Biosystems). Real-time qPCR was performed using a sequence detection system (Abi Prism 7500, Applied Biosystems) with SYBR Green (TaKaRa Bio). The primers are listed in Table S6.

2.4 | Western blotting, immunoprecipitation, and co-immunoprecipitation

These relevant protocols were performed as described previously.²⁹ For western blotting, cell and tissue samples were homogenized in RIPA lysis buffer (Santa Cruz Biotechnology). The protein concentration was determined using a bicinchoninic acid (BCA) Protein Assay Kit (Thermo Fisher Scientific). Proteins were separated by electrophoresis on 10% or 15% SDS-PAGE gels, and then transferred to nitrocellulose membranes. The membranes were blocked, incubated with the indicated antibodies, and then incubated with anti-rabbit or anti-mouse IgG secondary antibodies conjugated to horseradish peroxidase (HRP). Protein bands were detected using enhanced chemiluminescence and a digital imager (Tanon 5200; Biotanon). For immunoprecipitation and co-immunoprecipitation, the cells were washed twice with cold PBS and resuspended in RIPA lysis buffer containing 1 mM MgCl₂. After centrifugation, the supernatant was incubated with the indicated antibodies and Protein A/G PLUS agarose (sc-2003; Santa Cruz Biotechnology) in the presence of benzonase (1 U/mL, E1014; Sigma) overnight at 4°C. The beads were centrifuged, washed with washing buffer, and then boiled in SDS loading buffer for SDS-PAGE. The indicated antibodies are listed in Table S6.

2.5 | IHC staining and scoring criteria

IHC staining was performed as described previously.^{15,16} Tissue samples from 104 IMPC and 105 IDC patients who underwent surgery

between 2010 and 2012 and for whom complete clinical information was available were collected from the tissue specimen database of the Breast Cancer Prevention and Treatment Center of the Cancer Hospital of Tianjin Medical University. All samples were fixed in formalin and embedded in paraffin, and serial sections of tumor tissues were stained using standard H&E and IHC procedures. Two senior pathologists independently evaluated the immunohistochemically stained tissue in a double-blind manner. The levels of PRMT3 (1:100, ab240322; Abcam), H4R3me2a (1:100, PA5-102612; Invitrogen), RRBP1 (1:100, ab95983; Abcam), HSP90B1 (1:100, #20292; Cell Signaling Technology), ATF6 (1:100, ab227830; Abcam), HSPA5 (1:100, #31775; Cell Signaling Technology), and ADD1 (1:100, ab40760; Abcam) were evaluated according to the intensity and percentage of tumor cell staining. The dyeing intensity was classified as 0 (no staining), 1 (weak), 2 (moderate), and 3 (intense). The percentage of positive tumor cells was graded as 0 (<5%), 1 (6–25%), 2 (26–60%), and 3 (61–100%). The H score was calculated using the formula: H score = $\sum (i+1) \times P_i$, where i is the staining intensity of tumor cells (0–3), and P_i is the percentage of tumor cells stained within each intensity classification. The cutoff value was set to 150% for the H score. Samples with an intensity equal to or more than 150% are considered to have high PRMT3 expression; otherwise, they are considered to have low PRMT3 expression.

2.6 | Cell culture

MCF10A, HCC1937, MDA-MB-231, MCF7, T47D, BT474, and SKBR3 cell lines were purchased from the ATCC. The HCC1937, MDA-MB-231, MCF7, T47D, BT474, and SKBR3 cell lines were maintained in Dulbecco's modified Eagle's medium (DMEM, 06-1055-57-1ACS; Biological Industries) with 10% fetal bovine serum (FBS, 04-001-1ACS; Biological Industries) and 100 U/mL penicillin–streptomycin. MCF10A cells were maintained in DMEM/F12 (1:1) containing 5% horse serum, 0.5 µg/mL hydrocortisone, 10 µg/mL insulin, 20 ng/mL EGF, 0.1 µg/mL cholera toxin, and 100 U/mL penicillin–streptomycin. The MDA-MB-231 cells were treated with SGC707 (MCE, HY-19715) at concentrations of 4 and 8 µmol/L.

2.7 | Lentivirus packaging and infection

Before lentivirus infection, a PLKO.1 RNA interference vector or pSin overexpression vector and psPAX2 and pMD2.G plasmid were cotransfected into HEK293T cells at a ratio of 2:2:1 using Lipofectamine 2000 (11,668,027; Thermo Fisher Scientific). Lentiviruses were collected 48 and 96 hours post-transfection. MDA-MB-231, HCC1937, and MCF10A cells were infected with lentiviruses expressing shPRMT3 or FLAG-PRMT3 for 24 h in the presence of polybrene (4 µg/mL; Sigma–Aldrich), selectively cultured with puromycin for 48 h to eliminate untransduced cells, and then collected for analysis at a specified time point. For rescue experiments,

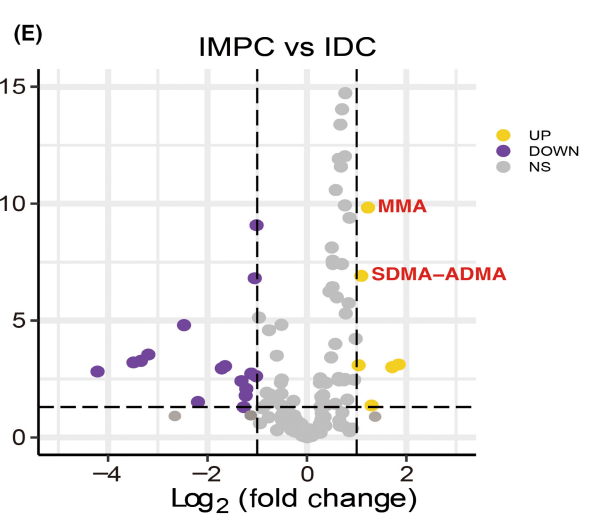
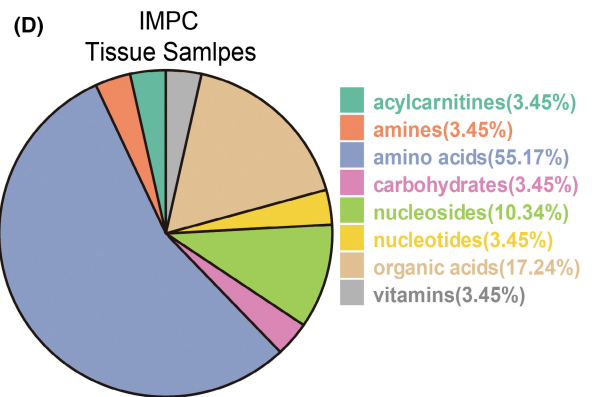
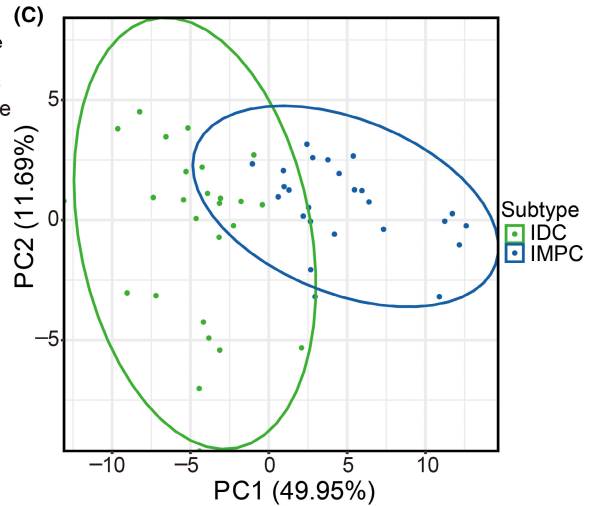
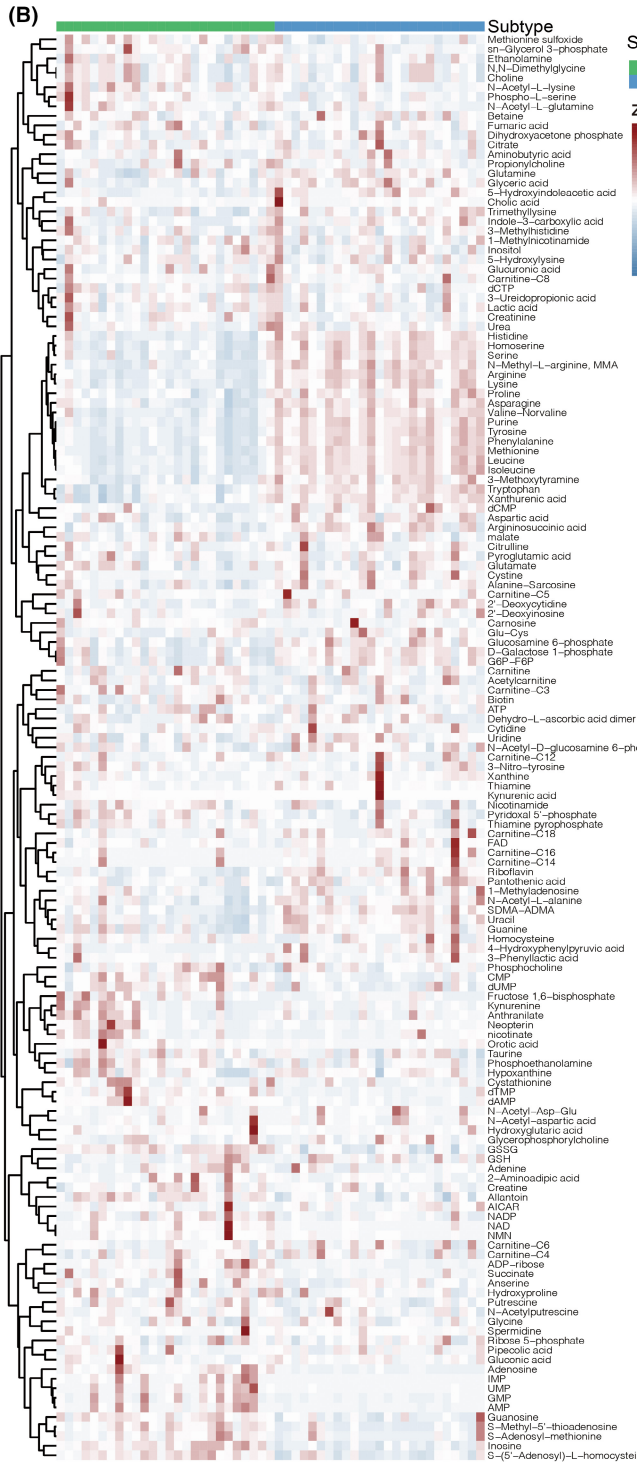
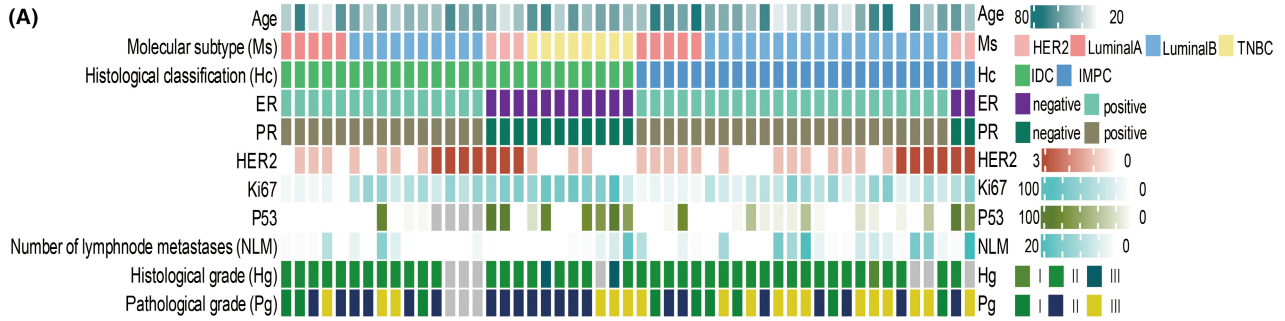


FIGURE 1 Metabolomic profiling of invasive ductal carcinoma and invasive micropapillary carcinoma. (A) Clinical parameters of the patient cohort are indicated in the heatmap. ER, estrogen receptor; PR, progesterone receptor; HER2, human epidermal growth factor receptor 2; Luminal A, ER-positive, PR-positive, HER2-negative; Luminal B, ER-positive, PR-negative, HER2-negative; TNBC, triple-negative breast cancer, ER-negative, PR-negative, HER2-negative. (B) Heatmap showing 149 profiled metabolites in invasive ductal carcinoma (IDC) and invasive micropapillary carcinoma (IMPC). (C) Principal component analysis (PCA) of tumor tissue from IDC (green) and IMPC (blue) samples based on metabolomics data. (D) Classes and counts of the metabolites detected in IMPC. (E) Volcano plots showing significantly differential metabolite in IMPC versus IDC. Arginine methylation-associated N^G -monomethylarginine (MMA), asymmetric N^G , N^G -dimethylarginine (ADMA), and symmetric N^G , N^G -dimethylarginine (SDMA) were the most significantly upregulated genes in IMPC. Wilcoxon rank-sum test, p -value <0.05 and fold change >2 or <0.5

PLKO.1 shRNA targeting sites within the 3'UTR of *PRMT3* was used to knock down its endogenous expression, and then the recombinant *PRMT3* gene containing coding sequence (CDS) regions was cloned into a pSin expression vector to knock in *PRMT3*. The shRNA targeting sequences are listed in [Table S6](#).

2.8 | Cell proliferation

Treated cells were plated into 6-well plates at a density of 5×10^4 cells or 1×10^4 cells. Cell numbers were counted using a Thermo Count II cell counter according to the manufacturer's instructions.

2.9 | Wound-healing test

A wound-healing test was performed as described previously.²⁰ MDA-MB-231 cells were plated into 6-well plates with 3×10^5 cells per well, cultured with the inhibitor SGC707 (4 and 8 $\mu\text{mol/L}$), and scraped with a 10- μl pipette tip. Wound closure was measured at different time points, and three random visual fields were recorded. The migration distance was analyzed using NIH ImageJ software.

2.10 | In vivo experiment

Four-week-old female BALB/c nude mice were purchased from Shanghai Shrek Experimental Animal Co., Ltd., and maintained in the Animal Experimental Center of Tianjin Medical University under specific-pathogen-free conditions. For the xenograft model, 5×10^5 infected breast cancer cells were resuspended in 50 μl of aseptic PBS and directly injected into the mammary gland fat pad of mice (five nude mice in each group). For the SGC707 treatment experiment, 5×10^5 infected breast cancer cells in 50 μl of aseptic PBS were directly injected into the mouse mammary gland fat pad in situ. SGC707 (30 mg/kg) was given by intraperitoneal injection every day for 40 days. To establish a mouse metastatic model, 5×10^5 infected breast cancer cells were resuspended in 50 μl of aseptic PBS and injected through the tail vein. Tumor growth was measured every 5 days for a period of 40 days post-implantation. The tumor volume was calculated using the formula $V = L \times W^2 / 2$ (V , volume; L , length; W , width of tumor).

2.11 | Mass spectrometry for PRMT3-associated proteins

The *PRMT3* protein was overexpressed in the MDA-MB-231 cells. In the presence of benzonase (E1014; Sigma), *PRMT3*-associated proteins were purified with anti-FLAG (M2) agarose beads and eluted with 3 \times FLAG peptide. Part of the elute was separated on SDS-PAGE gels and observed using silver staining. The remaining part was sent to Novogene for LC-MS/MS analysis.

2.12 | RNA sequencing

Three independent replicates of total RNA were isolated using TRIzol reagent (Invitrogen) from sh*PRMT3* MDA-MB-231 cells or shGFP MDA-MB-231 cells. The purity and integrity of total RNA were confirmed by Novogene. Sequencing analysis of expressed RNAs was carried out using an Illumina next-generation sequencing platform and sequenced reads were mapped to the hg38 human genome database. The *edgeR* R package (3.4) was used to analyze the sequencing count data to identify differentially expressed genes (DEGs) with a threshold of $p < 0.05$ and absolute fold change >1 between different groups. The biological functions of DEGs were analyzed with annotation databases (Gene Ontology [GO] and KEGG pathway databases) performed using the *clusterProfiler* R package. GO terms and KEGG pathways with a p -value < 0.05 were considered to be significantly enriched with DEGs. Gene set enrichment analysis (GSEA) was performed using the Java GSEA package. The list of genes annotated as GO or KEGG genes was obtained from The Molecular Signatures Database (MSigDB).

2.13 | Chromatin immunoprecipitation (ChIP) sequencing and ChIP-qPCR

Chromatin extraction and ChIP assays were performed as described previously.²⁹ In total, 1×10^7 cells were fixed with 1% formaldehyde (Sigma-Aldrich), lysed, and sonicated to generate chromatin fragments of between 200 and 600 bp in length. Chromatin was incubated with the indicated antibodies and protein A/G beads at 4°C overnight. Immunoprecipitated DNA was reverse cross-linked and digested with protein-K (Vazyme) at 65°C. DNA was purified using phenol/chloroform extraction. The purified DNA was adopted for

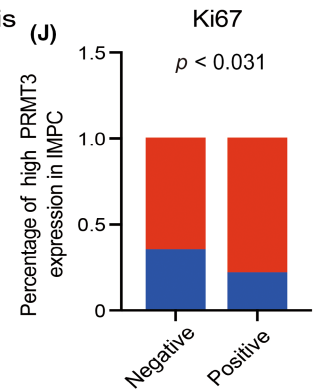
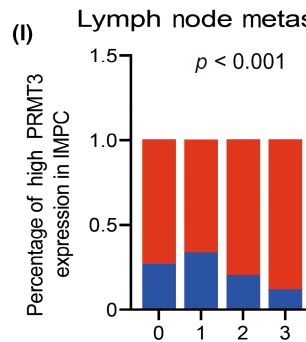
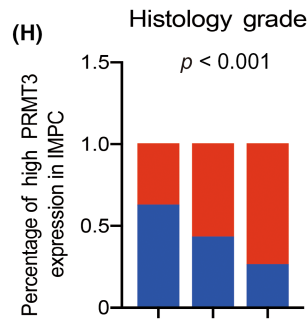
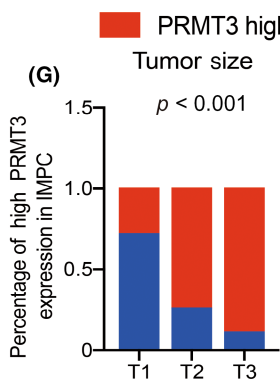
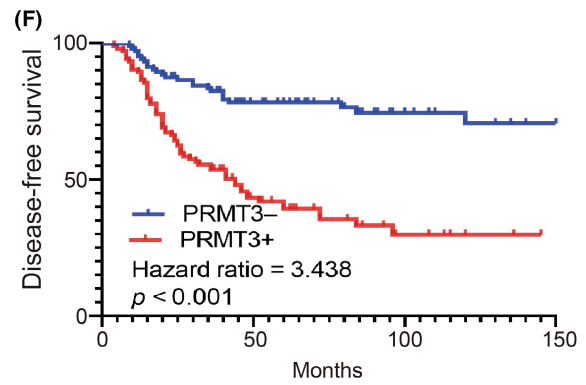
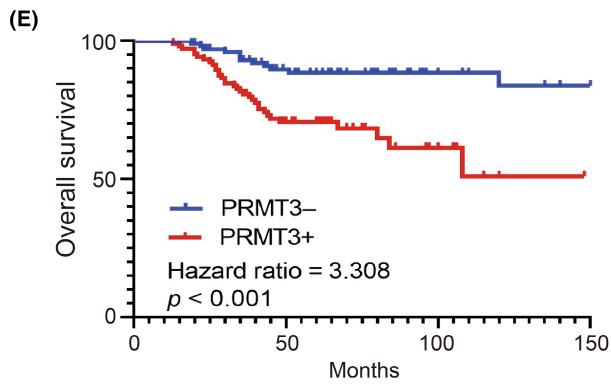
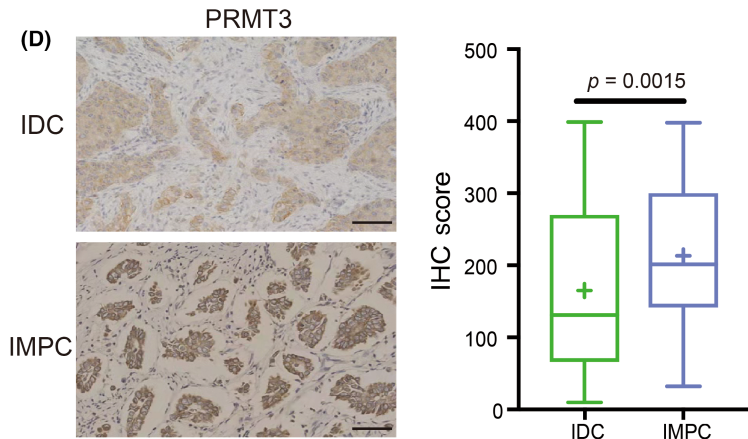
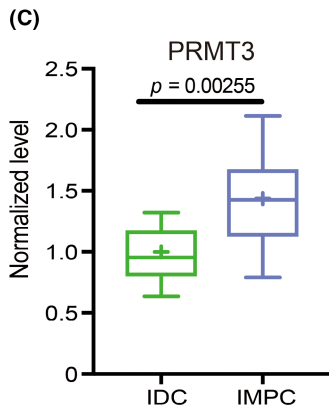
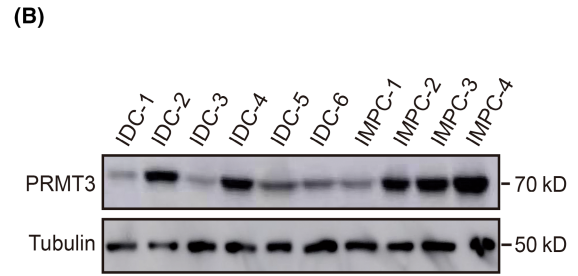
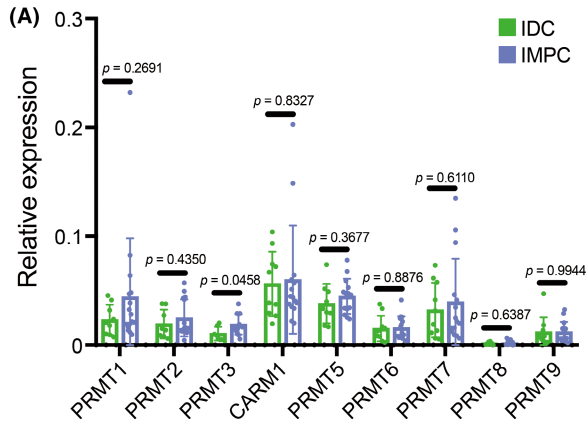


FIGURE 2 PRMT3 expression of IMPC patients and their clinicopathologic correlations. (A) mRNA expression of protein arginine methyltransferase (PRMT) family members normalized to the expression of GAPDH in IMPC and IDC patients ($n = 13$ for IMPC, and $n = 11$ for IDC). (B) Western blots showing the levels of PRMT3 in tumor samples from IMPC and IDC patients. (C) The quantification of PRMT3 protein in tumor samples from IMPC and IDC patients ($n = 13$ for IMPC, and $n = 11$ for IDC). The centerline and crossline represent the median and mean, respectively. The box bounds represent the interquartile range. The whiskers represent the lowest (or highest) data within 1.5 interquartile range. (D) Representative IHC images and IHC score of PRMT3 from patients in IMPC ($n = 104$) and IDC ($n = 105$). PRMT3 protein was confirmed as it was brown in an IHC assay performed with an anti-PRMT3 antibody. More intense brown staining was observed in IMPC. Scale bars indicate 100 μm . The centerline and crossline represent the median and mean, respectively. The box bounds represent the interquartile range. The whiskers represent the lowest (or highest) data within 1.5 interquartile range. (E, F) Kaplan–Meier curves showing association of PRMT3 expression with clinical prognosis, including overall survival (E) and disease-free survival (F), in IMPC patients (red represents a high PRMT3 expression level) (log-rank test; p -value < 0.001). (G–J) Percentages of high PRMT3 expression correlated with tumor size (G), histology grade (H), lymph node metastasis (I) and Ki67 expression (J) were examined using the Pearson χ^2 test. The data are presented as the mean \pm SD, and two-tailed Student's t -test was used

library preparation using a VAHTS Universal Plus DNA Library Prep Kit for Illumina (Vazyme). The quality of the library was determined with an Agilent 2100 Bioanalyzer and sequenced on an Illumina NovaSeq 6000 platform (Novogene). The raw data were processed with FASTP (0.22.0) to remove adapters and low-quality reads and then aligned to the hg38 human genome database using Bowtie (2.3.4.1) with default parameters. Unmapped reads, low-quality reads, and duplicated reads were removed using SAMtools (1.9) and Picard (2.23.3). Normalized bigwig was produced by deeptools (3.5.1). macs2 (2.2.6) was used to call peaks with a threshold of $p < 0.05$, and the ChIPseeker R package (1.24.0) was used to annotate peaks. For ChIP-qPCR, we analyzed the resultant DNA using SYBR Green Mix on the CFX Connect Real-Time PCR detection system (Bio-Rad). The primers of target gene promoters are listed in Table S6.

2.14 | Statistical analysis

We described the quantification and statistical methods for metabolomic analyses and all experiments in the figure legends and corresponding method subsections. All analyses were conducted using either GraphPad Prism or R. The clinicopathological characteristics were examined using Pearson χ^2 test and Fisher's exact test. Survival analysis was examined using Kaplan–Meier methods and log-rank test. Specifically, for nonparametric data, a two-sided Wilcoxon rank-sum test was used to compare two unpaired groups; for parametric data, two-tailed Student's t -test was used to compare two independent groups. A p -value < 0.05 was considered statistically significant.

3 | RESULTS

3.1 | The metabolomic landscape of IMPC showed a significant increase in arginine methylation marks

To obtain a comprehensive metabolomics profile of resected lesions obtained from our cohort of chemotherapy-naïve IDC ($n = 26$) and IMPC ($n = 25$) patients, we performed a targeted liquid chromatography–mass spectrometry (LC–MS)-based metabolomic analysis (Figure S1A). The clinical characteristics of the patients are shown in Figure 1A and

Table S1. We detected 149 metabolites in the tissue samples (Table S2), and a clustering analysis and PCA revealed distinct metabolic profiles between IDC and IMPC (Figure 1B,C). Indeed, the global distribution of metabolic classes in IMPC was the most highly enriched with amino acids, at 55.17%, followed by organic acids (17.24%), nucleosides (10.34%), nucleotides (3.45%), carbohydrates (3.45%), and ~10–11% metabolites of other types, whereas the vast majority of metabolites in IDC were in the nucleotide class (Figures 1D, S1B). Moreover, we identified 20 significantly differential metabolites in IMPC versus IDC (14 with decreased and 6 with increased abundance; Wilcoxon rank-sum test, p -value < 0.05 and fold change > 2 or < 0.5). Notably, a marked elevation in the arginine methylation-associated metabolites MMA and ADMA-SDMA was found in the IMPC patients compared with the IDC group (Figure 1E; Table S3). In addition, the most significantly down-regulated metabolites in IMPC were GSSG, inosine, and adenosine, which are related to glutathione metabolism and purine metabolism, respectively (Table S3). However, glutathione metabolism and purine metabolism have been reported to be enhanced in tumor cells, in which elevated levels promote tumor progression.^{30,31} Furthermore, a KEGG pathway-based analysis showed that arginine biosynthesis and metabolism pathways were significantly upregulated in IMPC (Figure S1C). The levels of arginine, MMA, and ADMA-SDMA were higher in tumor samples from IMPC patients than those from IDC patients (Figure S1D). Taken together, the aberrant arginine methylation might be highly involved in the malignant biological behaviors of IMPC. Here, we concentrated on arginine methylation because it is a crucial regulator of processes seized by cancer cells to ensure survival.^{21,22}

3.2 | High levels of PRMT3 are positively correlated with poor prognosis in IMPC patients

We next investigated the levels of nine PRMTs in our patient cohort and found that only *PRMT3* mRNA was significantly upregulated in tumor samples from IMPC compared with those from IDC (Figure 2A). Consistently, higher PRMT3 protein levels were observed in the IMPC group than in the IDC group (Figures 2B,C, S2A). Furthermore, tumor samples from 209 patients ($n = 105$ with IDC and $n = 104$ with IMPC) were used to detect PRMT3 expression by IHC staining. Greater PRMT3 expression was observed in

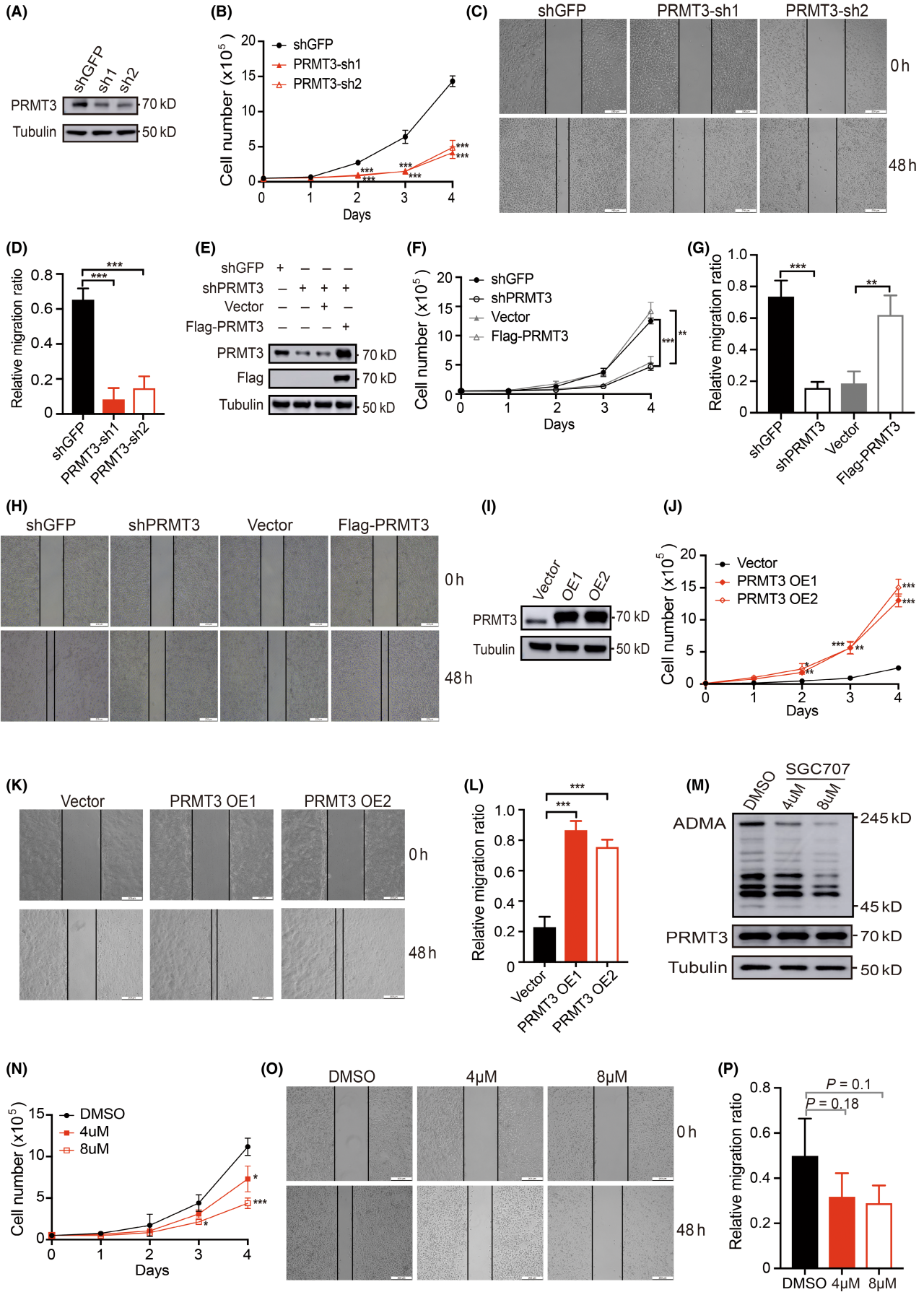


FIGURE 3 PRMT3 promoted breast cancer cell proliferation and invasion in vitro. (A) MDA-MB-231 cells after PRMT3 knockdown were collected, and the PRMT3 protein levels were determined using western blot analysis. (B) Cell proliferation of MDA-MB-231 cells and PRMT3-knockdown MDA-MB-231 cells at the indicated time. (C, D) Representative image showing wound healing at 0 and 48 h (C) and quantitative analysis of the migration distance of the MDA-MB-231 cells transfected with an empty vector and PRMT3 shRNAs (D). (E) MDA-MB-231 cells stably transfected with shRNA constructs were transiently transfected with the expression vectors encoding either pSin (Vector) or recombinant PRMT3 gene (Flag-PRMT3) and the resulting cells were analyzed by western blotting. (F) Cell proliferation for control and PRMT3 knockdown MDA-MB-231 cells with or without knock-in PRMT3. (G, H) Quantitative analysis (G) and representative image (H) of the migration distance for control and PRMT3 knockdown MDA-MB-231 cells with or without knock-in PRMT3. (I) MCF10A cells derived from nontumorigenic epithelial cells after PRMT3 overexpression were collected, and the PRMT3 protein levels were determined by western blot analysis. (J) Cell proliferation of MCF10A cells and PRMT3-overexpression MCF10A cells at the indicated time. (K, L) Representative image showing the wound-healing assay at 0 and 48 h (K) and quantitative analysis of the migration distance of MCF10A cells transfected with an empty vector and Flag-PRMT3-WT (L). (M) Effect of treating MDA-MB-231 cells with the PRMT3 inhibitor SGC707 was shown by immunoblotting for panasymmetric dimethylarginine (ADMA) detection. (N) Cell proliferation of MDA-MB-231 cells treated with SGC707 (4 μ M) and SGC707 (8 μ M) at the indicated time. (O, P) Representative image showing the wound-healing assay at 0 and 48 h (O) and quantitative analysis of the migration distance of MDA-MB-231 cells treated with SGC707 (P). Scale bars = 200 μ m. The data are presented as the mean \pm SD of three independent experiments. * p < 0.05, ** p < 0.01, *** p < 0.001 (two-tailed Student's *t*-test).

the IMPC samples, whereas weaker IHC staining was observed in the IDC samples (Figures 2D, S2B; Table S4). To further assess the clinical relevance of PRMT3 in IMPC, we analyzed the correlation of PRMT3 expression with the overall survival (OS) and disease-free survival (DFS) of 104 IMPC patients. Patients with IMPC and high levels of PRMT3 showed a decreased OS and DFS compared with patients with IMPC and low levels of PRMT3 (Figure 2E,F). In addition, we explored the clinicopathological characteristics of 104 IMPC patients with high or low levels of PRMT3 (Table S5). The data showed that high PRMT3 expression was positively correlated with tumor size, histological grade, lymph node metastasis, and the proliferative marker Ki67 (Figure 2G–J), but the levels of PRMT3 were not related to estrogen receptor (ER), progesterone receptor (PR), or human epidermal growth factor receptor 2 (HER2) (Figure S3A–C). Subsequently, we explored the association between PRMT3 expression and breast cancer progression based on a dataset of metastatic breast cancer from The Cancer Genome Atlas (TCGA). Notably, TCGA data showed typically high PRMT3 expression levels in metastatic breast cancer tissues relative to nontumor tissues (p -value = 1.93e-11; Figure S3D). Correlation analysis showed a weak association between the high expression of PRMT3 and the breast cancer metastasis-related genes cyclin D1, MYC,^{32,33} and Ki67 (Figure S3E–G). These results demonstrated a clear relationship between PRMT3 and the clinical aggressiveness of IMPC.

3.3 | PRMT3 regulates cell proliferation and migration in vitro

Next, we detected the expression of PRMT3 in multiple breast cancer cell lines. The PRMT3 levels in MDA-MB-231, HCC1937, MCF7, and T47D cells were increased relative to those in MCF10A cells, which are derived from nontumorigenic breast epithelial cells, at both the transcript and protein levels (Figure S4A,B). We used the MDA-MB-231 and HCC1937 aggressive breast cancer cell lines to establish PRMT3 knockdown by cotransduction of lentivirus encoding short hairpin RNAs (shRNAs) specific to PRMT3 (Figures 3A, S4C). Downregulation of PRMT3 expression via shRNAs significantly

decreased the proliferation of both MDA-MB-231 and HCC1937 cells relative to control cells (Figures 3B, S4D). In the PRMT3 shRNA groups, the migration distance of the MDA-MB-231 and HCC1937 cells at 48 h was significantly reduced relative to that of the control cells (Figures 3C,D, S4E,F). To test whether the re-expression of PRMT3 rescued the knockdown phenotype, we transfected the expression vector encoding recombinant PRMT3 gene into PRMT3-knockdown MDA-MB-231 and HCC1937 cell lines (Figures 3E, S4G). Restoration of PRMT3 resulted in markedly increased cell proliferation and migration, essentially like control cells (Figures 3F–H, S4H–J). Furthermore, we generated PRMT3-overexpressing MCF10A cell lines (Figure 3I). As shown in the cell growth curve, PRMT3 overexpression promoted the proliferation of wild-type MCF10A cells (Figure 3J). The cell migration distance showed a significant increase in PRMT3-overexpressing MCF10A cells compared with control cells (Figure 3K,L). In addition, we followed the growth and migration of MDA-MB-231 cells after treatment with the PRMT3 inhibitor SGC707. The production of ADMA catalyzed by PRMT3 was significantly reduced in a dose-dependent manner, but the PRMT3 levels were not changed (Figure 3M). Importantly, the PRMT3 inhibitor exerted a suppressive effect on the growth and migration of MDA-MB-231 cells (Figure 3N–P). PRMT1 has previously been reported to promote the proliferative and metastatic capabilities of breast cancer.^{25,34} To investigate whether PRMT3 exerts its molecular functions independently of PRMT1, we established PRMT1-knockdown, PRMT3-knockdown, and double PRMT1- and PRMT3-knockdown MDA-MB-231 cell lines and analyzed their proliferation and migration. As expected, depletion of either PRMT1 or PRMT3 reduced cell growth and migration distance, while depletion of both PRMT1 and PRMT3 led to a further reduction in cell proliferation and migration (Figure S4K–N).

3.4 | PRMT3 was required for tumor growth and metastasis in vivo

To evaluate the role played by PRMT3 in breast cancer pathogenesis in vivo, we implanted shPRMT3 MDA-MB-231 or shPRMT3

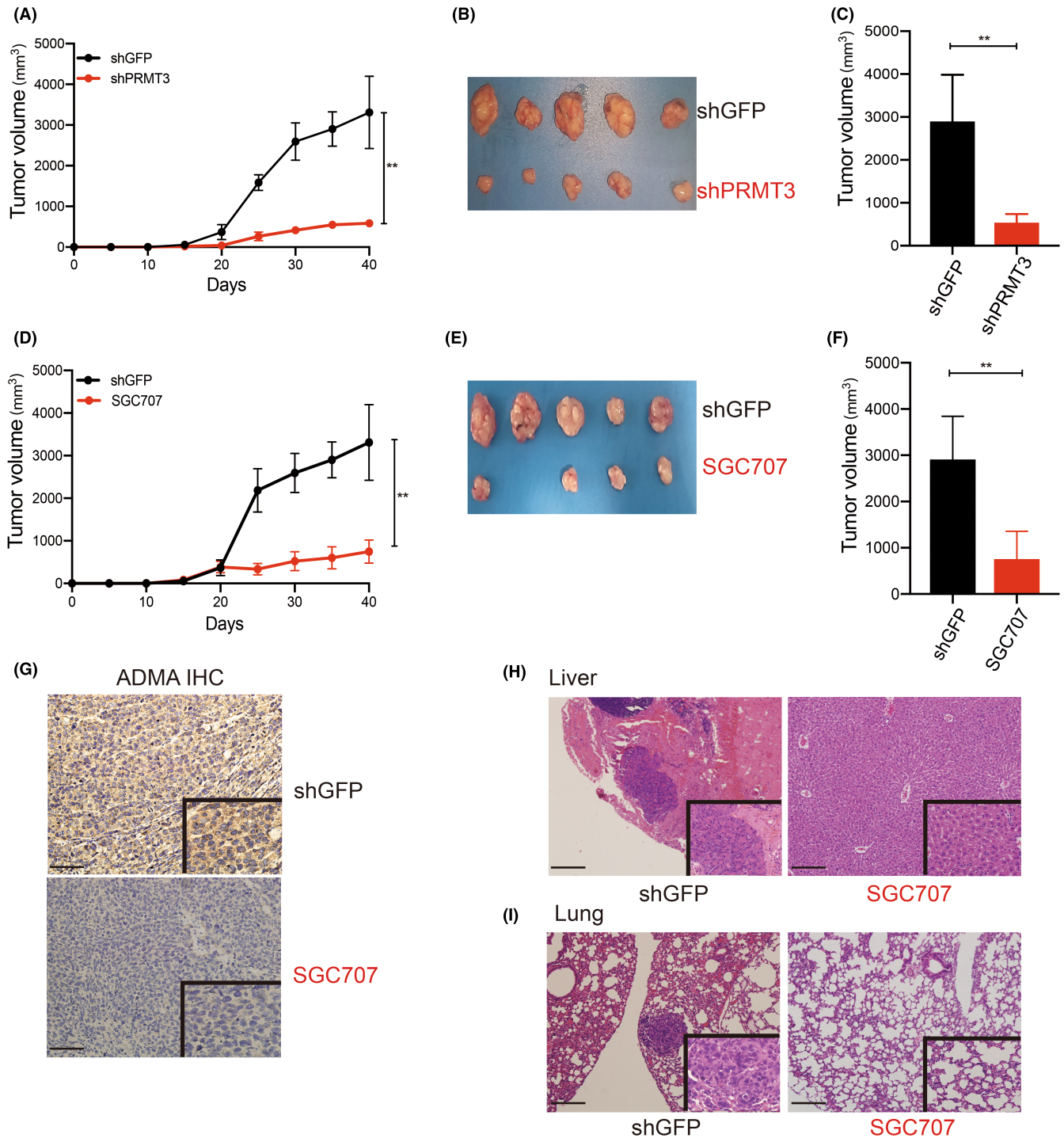


FIGURE 4 PRMT3 promoted the tumorigenic capacity of breast cancer cells in vivo. (A–C) shPRMT3 or shGFP MDA-MB-231 cells were directly injected into the mammary fat pad of female BALB/c nude mice ($n = 5$). Tumor growth was measured every 5 days for a period of 40 days post-implantation (A). Tumors were measured and isolated at the time of mouse sacrifice (B, C). (D–F) shGFP MDA-MB-231 cells were directly injected into the mammary fat pad of female BALB/c nude mice ($n = 5$) followed by treatment with the PRMT3 inhibitor SGC707. Tumor growth was measured every 5 days for a period of 40 days post-implantation (D). Tumors were measured and isolated at the time of mouse sacrifice (E, F). (G) Representative IHC images showing ADMA in the isolated tumor samples from mice. ADMA was confirmed to be a brown color in the IHC assays with anti-ADMA antibody. (H, I) To detect tumor metastasis after SGC707 treatment, female BALB/c nude mice ($n = 5$) were intravenously injected with shGFP MDA-MB-231 cells and treated with SGC707. Representative images of H&E showing an obvious reduction in liver (H) and lung (I) metastatic foci. Scale bars indicate 100 μm . The data are presented as the mean \pm SD. * $p < 0.05$, ** $p < 0.01$ (two-tailed Student's t -test)

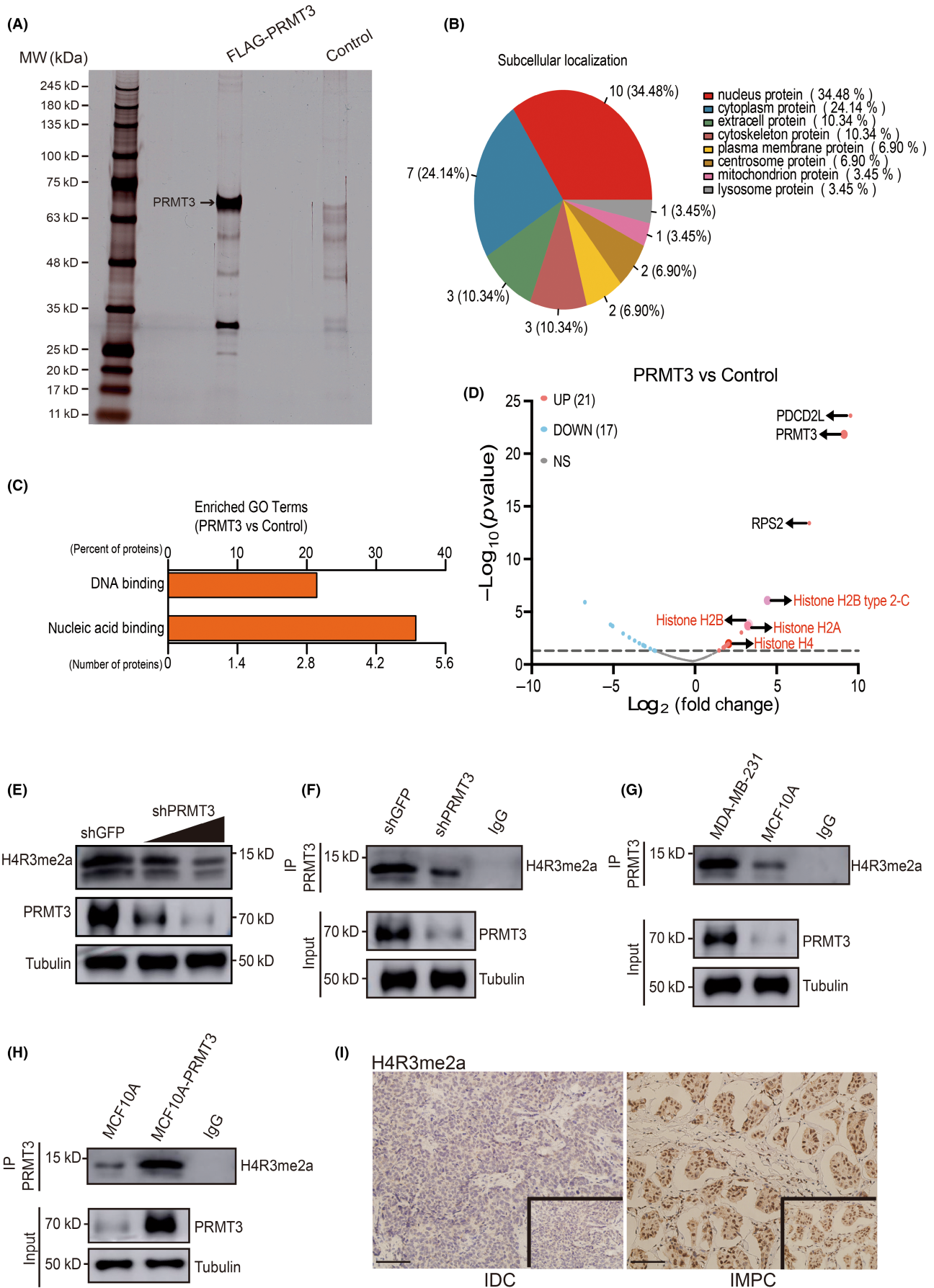


FIGURE 5 Legend on next page

FIGURE 5 PRMT3 increased H4R3me2a levels. (A) Factors associated with PRMT3 in silver-stained gel. The arrow denotes FLAG-tagged PRMT3 in the silver-stained gel. MW, molecular weight. (B) Subcellular localization analysis showing that PRMT3-binding proteins were mainly nuclear proteins. Extracts from MDA-MB-231 cells ectopically expressing FLAG (Ctrl) or FLAG-PRMT3 were purified with anti-FLAG M2 beads and eluted with the FLAG peptide. The elution was analyzed by mass spectrometry. (C) GO annotation of PRMT3-associated proteins demonstrated that DNA binding and nucleic acid binding were significantly high ($p < 0.05$). (D) Volcano plot showing significantly differentially interacting proteins ($p < 0.05$ and fold change > 2 or < 0.5) in the PRMT3 group versus the control group. (E) PRMT3 knockdown suppressed H4R3me2a in MDA-MB-231 cells. (F) PRMT3 knockdown decreased the association of H4R3me2a with PRMT3 in MDA-MB-231 cells. (G) Association of H4R3me2a with PRMT3 in MDA-MB-231 cells was significantly increased compared with that in MCF10A cells. (H) Forced expression of PRMT3 enhanced the association of H4R3me2a with PRMT3 in MCF10A cells. (I) Representative images showing H4R3me2a expression in IMPC and IDC tumor samples. Scale bars = 100 μm .

HCC1937 cells into female BALB/c nude mice. We observed that PRMT3-depleted tumors showed dramatic decreases in final tumor volume and tumor growth rate (Figures 4A–C, S5A–C). To explore the clinical relevance of the PRMT3 inhibitor, we treated nude mice injected with shGFP MDA-MB-231 cells with SGC707, a specific inhibitor of PRMT3, and found that tumor growth was significantly suppressed by the inhibitor (Figure 4D–F). The tumor samples also showed decreased levels of ADMA after SGC707 treatment (Figure 4G). In addition, mice not treated with SGC707 exhibited cachexia, as indicated by weight loss and multiple macroscopic metastatic foci, whereas mice treated with SGC707 showed significant attenuation of this phenotype (Figure S5D,E). A histological examination revealed that mice bearing shGFP-expressing MDA-MB-231 cells had developed noticeable liver and lung metastases (Figure 4H,I). In contrast, SGC707 treatment substantially inhibited tumor cell metastasis (Figure 4H,I). Together, these data strongly suggested that PRMT3 plays an oncogenic role in vivo and that PRMT3 inhibitors are promising therapeutic treatments for human breast cancer.

3.5 | PRMT3 increases the levels of H4R3me2a

To elucidate the potential molecular mechanisms by which PRMT3 overexpression may enhance breast cancer progression in vitro and in vivo, we performed affinity purification combined with mass spectrometry with FLAG-tagged PRMT3-overexpressing MDA-MB-231 cells to identify PRMT3 substrate specificity (Figure 5A). In addition to programmed cell death 2-like (PDCD2L) and 40S ribosomal protein S2 (RPS2), two known substrates of PRMT3,^{35,36} PRMT3-associated proteins were mainly nuclear proteins, as revealed by mass spectrometry analysis (Figure 5B). Notably, a GO analysis of molecular function implicated PRMT3-associated proteins in DNA binding and nucleic acid binding; these substrates included histone H4, histone H2A, histone H2B, and histone H2B type 2-C (Figure 5C,D). Type I arginine methyltransferases regulate the asymmetric demethylation of the third arginine residue on histone H4 (H4R3me2a) to promote gene expression, and aberrant H4R3me2a has been linked to cancer.^{37,38} Therefore, we speculated that PRMT3 promoted the H4R3me2a modification. Western blotting revealed that PRMT3 knockdown led to a dose-dependent reduction in H4R3me2a levels in MDA-MB-231 cells,

implying that PRMT3 is a potential regulator of histone H4 arginine methylation (Figure 5E). This interaction appears direct and bona fide, as a co-IP assay confirmed that the H4R3me2a level was regulated by exogenously overexpressed PRMT3 in normal breast epithelial cells (MCF10A cells) and by endogenous PRMT3 knockdown in MDA-MB-231 cells (Figure 5F–H). Notably, the H4R3me2a level was significantly elevated in IMPC patients with high PRMT3 expression compared with the level in IDC patients (Figure 5I).

3.6 | PRMT3 regulated the ER stress signaling pathway

PRMTs epigenetically regulate gene expression.^{21,39} We hypothesized that a mechanism by which PRMT3 regulates breast cancer cell proliferation and invasion involves transcriptional control. To test this hypothesis, we transfected lentivirus-encoded shRNA specific to PRMT3 in MDA-MB-231 cells and performed RNA sequencing. Efficient PRMT3 knockdown induced a substantial change in the transcriptional profile, with the majority of genes showing downregulated expression ($n = 404$ genes were downregulated; $n = 195$ genes were upregulated significantly), which suggested that PRMT3 knockdown suppressed transcription (Figure 6A). Enrichment analysis of the 404 significantly downregulated genes based on the GO and KEGG database identified that several ER stress-related and UPR-related signaling pathways showed the most significant response to PRMT3 knockdown (Figures 6B, S6A). Assessing an MA plot of filtered DEGs to perform GSEA, we found that the UPR pathway was significantly downregulated in PRMT3-knockdown breast cancer cells (Figures 6C, S6B). A heatmap analysis also showed that PRMT3 knockdown significantly decreased the expression of UPR-related genes (Figure 6D). Consistent with this finding, the mRNA levels of UPR-related genes were downregulated by PRMT3 knockdown in MDA-MB-231 cells (Figure 6E). Because we demonstrated that PRMT3 facilitated the H4R3me2a modification, we hypothesized that PRMT3-activated ER stress was mediated mechanistically through increased H4R3me2a. To investigate this possibility, we performed ChIP sequencing to measure the genome-wide occupancy of H4R3me2a in MDA-MB-231 cells with PRMT3 knocked down or GFP knocked down. H4R3me2a was mainly localized around regions between a TSS and a TES, with a greater abundance near the TSS site (Figures 6F, S6C). H4R3me2a was localized around

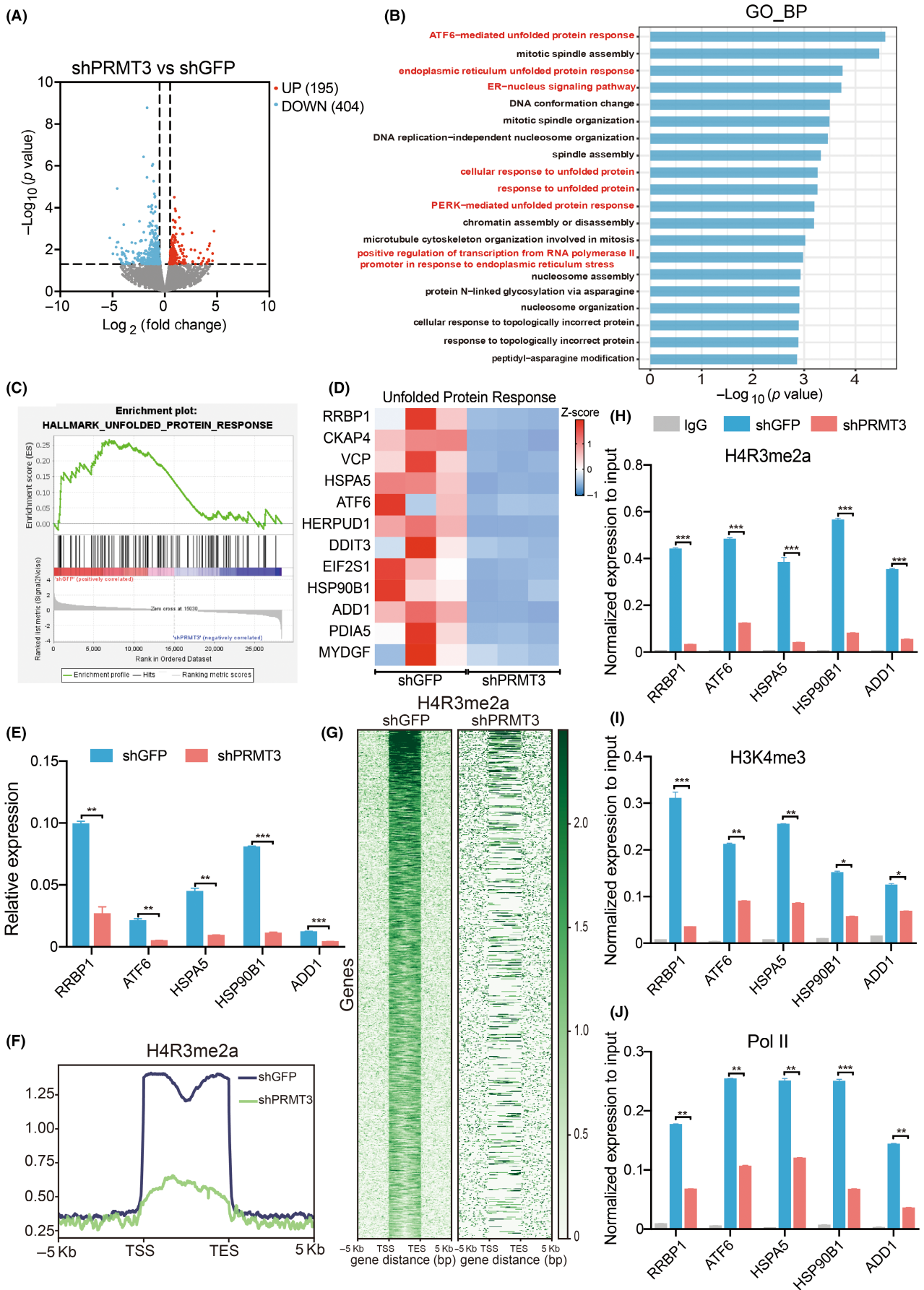
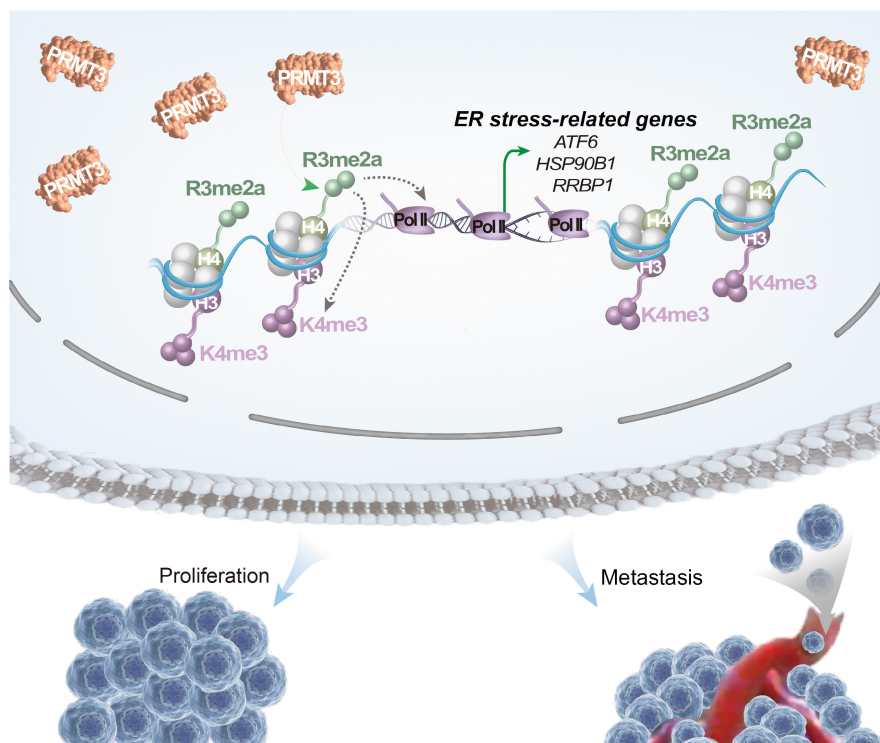


FIGURE 6 Legend on next page

FIGURE 6 PRMT3 regulated the endoplasmic reticulum stress signaling pathway. (A) Volcano plot showing RNA-seq data of differentially expressed genes (DEGs) between PRMT3-knockdown and GFP-knockdown MDA-MB-231 cells; 404 genes were downregulated, and 195 genes were upregulated (fold change >2 or <0.5 and $p < 0.05$). (B) For the analysis of PRMT3-knockdown-mediated transcription, GO analysis showed that endoplasmic reticulum stress and UPR-related signaling pathways (indicated with red letters) were the most significantly enriched. (C) A GSEA showing that PRMT3 knockdown led to UPR pathway downregulation. (D) Heatmap showing the gene set in UPR as identified by GSEA. (E) Real-time qPCR validation of UPR-related genes normalized to the expression of GAPDH in MDA-MB-231 cells. (F) Meta profile of the H4R3me2a ChIP-seq signal at the region between the TSS and TES in PRMT3-knockdown and GFP-knockdown cells. (G) Heatmap showing H4R3me2a signals within a window of 5 kb in the region between the TSS and the TES in PRMT3-knockdown and GFP-knockdown cells. (H–J) Enrichment of H4R3me2a (H), H3K4me3 (I) and Pol II (J) or rabbit IgG at ER stress-related gene promoters as determined by ChIP-qPCR. The data are presented as the mean \pm SD. * $p < 0.05$, ** $p < 0.01$, *** $p < 0.001$ (two-tailed Student's *t*-test).

FIGURE 7 PRMT3 promoted proliferation and metastasis in the breast cancer by promoting H4R3me2a and inducing ER stress. We propose a potential molecular mechanism by which PRMT3 plays a key role in promoting the proliferation and metastasis of cancer cells. The elevated expression of PRMT3 promotes H4R3me2a, which might increase H3K4me3 and Pol II localization to the promoter-proximal regions of ER stress-related genes to facilitate transcription.



the TSS of promoters and the regions from the TSS to the TES that exhibited a more marked reduction in PRMT3 knockdown compared with GFP knockdown (Figures 6F,G, S6C,D). PRMT3 knockdown caused a pronounced reduction in H4R3me2a signals at the genomic loci of ER stress-related genes (Figure S6E). Furthermore, ChIP-qPCR showed that PRMT3 knockdown significantly decreased the occupancy of H4R3me2a in the promoter region of ER stress-related genes (Figure 6H). H3K4me3 and Pol II, two markers known to promote gene transcription,⁴⁰ were significantly enriched in the promoter regions of ER stress-related genes, which was consistent with the changes in the H4R3me2a level (Figure 6H,I). Notably, the occupancy of H3K4me3 and Pol II localized at the promoter of ER stress-related genes seemed to depend on PRMT3 regulation of H4R3me2a occupancy (Figure 6H,I). These results suggested that the H4R3me2a modification regulated by PRMT3 was consistent with the functions of the classical histone modification H3K4me3 and Pol II, which drove ER stress-related gene expression. ER stress and UPR have been reported to promote the proliferation

and metastasis of tumor cells.^{41,42} Finally, we measured the levels of ER stress-related proteins in the tumor tissues from IMPC and IDC patients by IHC assays. These ER stress-related proteins were expressed at low levels in the IDC group, and higher expression levels were observed in IMPC patients with high PRMT3 expression (Figure S7A,B). Moreover, we observed that high PRMT3 expression positively correlated with ER stress-related protein expression in the IMPC group (Figure S7C).

4 | DISCUSSION

As much of the current understanding of the malignant biological behavior of IMPC is based on clinical investigations,^{43–46} the characterization of the metabolic reprogramming in IMPC is urgently needed to clarify the molecular mechanisms underlying its high invasive and metastatic behaviors and to establish a promising scientific basis for clinical treatment. In this study, targeted metabolomic

analysis of IMPC tumor samples followed by mechanistic verification analyses led to the following conclusions: (1) the metabolomic profile of IMPC revealed elevated arginine methylation; (2) PRMT3 was overexpressed in IMPC and elevated PRMT3 levels correlated with poor clinical prognosis; (3) PRMT3 was identified as a key molecule in regulating the proliferation and metastasis of breast cancer cells both *in vitro* and *in vivo*; (4) mechanistic studies demonstrated that PRMT3 might facilitate the occupancy of H3K4me3 and Pol II on ER stress-related genes by regulating H4R3me2a, promoting the proliferation and invasion of breast cancer cells (Figure 7).

Breast cancer, as a highly heterogeneous disease, is classified by different histological subtypes, clinical symptoms, and prognoses.⁴⁷ Metabolomics is a powerful tool for identifying cancer biomarkers and risk factors driving tumorigenesis and tumor progression.⁴⁸ To date, studies on metabolism in breast cancer have mainly focused on characterizing triple-negative breast cancer (TNBC) with high metastatic capacity and relatively poor prognosis.^{49,50} Compared with TNBC, IMPC has been reported to exhibit larger tumor volume, greater lymphovascular invasion, and lymph node involvement, and has led to a worse prognosis.⁵¹ However, few investigations into the metabolic profile of IMPC have been reported, possibly because the rare incidence of IMPC means that few tumor samples are available.⁴ A previously reported *in vivo* experiment confirmed that arginine deficiency significantly inhibited small-cell lung cancer proliferation and promoted mouse survival.⁵² Interestingly, arginine biosynthesis appears to play an important role in IMPC and TNBC. For example, ASL and NOS, two critical enzymes in arginine synthesis, are essential for maintaining the proliferation and invasion of TNBC cells.^{53,54} Although the metabolite changes related to ASL and NOS enzymes have not been identified in IMPC, high levels of arginine and arginine methylation products (MMA and ADMA-SDMA) were found in IMPC (Figure 1). Thus, we believe the biosynthesis and metabolism of arginine play important roles in the malignant progression of breast cancer.

PRMTs catalyze protein arginine methylation and exert molecular functions through epigenetically mediated gene transcription, regulation of the DNA damage response, and immune surveillance.²¹ A recent study showed that PRMT1 methylated the histone methyltransferase EZH2, promoting the metastasis of breast cancer cells.³⁴ In addition, PRMT5 recruits SET1 by catalyzing the symmetrical dimethylation of H3R2me2s to promote H3K4me3 localization at the FOXP1 promoter, maintaining the proliferation and self-renewal of breast cancer stem cells.⁵⁵ As studies have progressed, PRMTs have rapidly attracted interest as novel cancer drug targets. However, tumor-specific PRMT expression has rarely been studied. In this study, an analysis of a large number of tumor samples revealed high tissue-specific PRMT3 expression in IMPC (Figure 2), providing a novel direction for the accurate diagnosis and treatment of IMPC.

A recent discovery revealed that PRMT3 preferentially methylated histone H4 *in vitro*.⁵⁶ Consistent with this finding, we demonstrated with mass spectrometry analysis that PRMT3 interacted with histone H4 in MDA-MB-231 cells and facilitated H4R3me2a in a dose-dependent manner (Figure 5). H4R3me2a promotes

gene transcription by recruiting the MLL protein to promote the H3K4me3 modification.⁵⁷ H3K4me3 is an epigenetic modification that is widely found at promoter-proximal nucleosomes of protein-coding genes in a variety of cells, including breast cancer cells.^{58,59} H3K4me3 covers the majority of the genome and is positively correlated with gene transcription frequency.⁶⁰ Notably, our data confirmed that PRMT3 knockdown significantly reduced H4R3me2a at the promoter region (Figure S6C,D), which might attenuate MLL recruitment to decrease H3K4me3 modification, leading to repress gene expression. However, a heatmap analysis showing the distribution of H4R3me2a on full-length genes showed that PRMT3 knockdown not only reduced H4R3me2a near the promoter but also significantly reduced the H4R3me2a signals localized at the TES of genes (Figure 6F,G). Whether this effect changes gene transcription remains to be determined.

The ER stress response, also termed the UPR, is a mechanism that maintains endoplasmic reticulum homeostasis.⁴¹ Carcinogenic transformation requires the UPR to overcome a variety of obstacles.⁶¹ The sustained activation of the UPR ensures that cancer cells adapt to the high rate of protein synthesis to meet increased metabolic needs.⁴² Furthermore, metastatic foci caused by DTCs show high UPR activation. For example, activation of the UPR in breast and colon cancers induced dormancy in tumor cells by enabling their resistance to the harsh environments of distal organs.⁶² Our results showed that the knockdown of PRMT3 in breast cancer cells was accompanied by a decrease in the expression of UPR-related genes (Figure 6B-E), which suggested that PRMT3-mediated ER stress might be an important event in tumor growth and metastasis. Notably, we detected high levels of UPR-related proteins in IMPC patients that were positively correlated with high PRMT3 expression (Figure S7). Therefore, we speculated that PRMT3-mediated ER stress might be related to the high invasion and metastasis behaviors of IMPC, and we will explore this in follow-up research.

In summary, we identified a large-scale targeted metabolomics analysis of aberrant arginine methylation and elevated PRMT3 expression in IMPC. Significantly, our study revealed a novel potential regulatory mechanism in which PRMT3 promoted the proliferation and metastasis of breast cancer cells through the regulation of H4R3me2a and ER stress, which provides a valuable reference for clinical intervention and diagnosis. However, whether this pathway can be adopted as a widely applicable mechanism for IMPC and other highly metastatic breast cancers remains to be determined.

AUTHOR CONTRIBUTIONS

R.Z., K.W., S.L., and L.F. designed the study and collected clinical samples. R.Z. performed *in vitro* experiments, immunoprecipitation, western blot, qPCR, RNA-seq, ChIP-seq, ChIP-qPCR, and bioinformatic analysis. K.W. performed *in vivo* experiments, and immunohistochemical and pathological analyses. R.Z., K.W., J.Z., H.L., and C.N. performed statistical analysis, data analysis, and data verification. S.L. and L.F. supervised the whole study. R.Z. wrote the paper. All authors reviewed the manuscript and approved the manuscript prior to submission.

ACKNOWLEDGMENTS

We thank Professor Zeping Hu from Tsinghua-Peking Center for Life Sciences for targeted metabolomic analysis. We thank Professor Deqing Hu from Tianjin Key Laboratory of Medical Epigenetics for his technical assistance.

FUNDING INFORMATION

This study was supported by grants from the National Natural Science Foundation of China (nos. 82173344, 81872164, and 31870860).

CONFLICT OF INTEREST

The authors have no conflict of interest.

DATA AVAILABILITY STATEMENT

The data used to support the findings of this study are included in the article. All other data supporting the findings of this study will be made available upon reasonable request to the corresponding authors.

ETHICS STATEMENT

Approval of the research protocol by an Institutional Reviewer Board: The protocol for the research project was approved by the Ethics Committee of Tianjin Medical University Cancer Institute and Hospital (Institutional Review Board: bc2019075).

Informed Consent: N/A.

Registry and the Registration No. of the study/trial: N/A.

Animal Studies: Experiments with mice were approved by the Committee for Animal Experimental Center of Tianjin Medical University (TMUaMEC2021016).

INFORMED CONSENT

Written informed consent was obtained from each patient.

ORCID

Renyong Zhi  <https://orcid.org/0000-0003-1059-9339>

REFERENCES

- Sung H, Ferlay J, Siegel RL, et al. Global cancer statistics 2020: GLOBOCAN estimates of incidence and mortality worldwide for 36 cancers in 185 countries. *CA Cancer J Clin*. 2021;71(3):209-249.
- Bocker W. WHO classification of breast tumors and tumors of the female genital organs: pathology and genetics. *Verh Dtsch Ges Pathol*. 2002;86:116-119.
- Luna-More S, Gonzalez B, Acedo C, Rodrigo I, Luna C. Invasive micropapillary carcinoma of the breast. A new special type of invasive mammary carcinoma. *Pathol Res Pract*. 1994;190(7):668-674.
- Yang YL, Liu BB, Zhang X, Fu L. Invasive micropapillary carcinoma of the breast: an update. *Arch Pathol Lab Med*. 2016;140(8):799-805.
- Kuroda N, Hamaguchi N, Ohara M, Hirouchi T, Miyzaki E, Mizuno K. Intracytoplasmic lumina in invasive micropapillary carcinoma of the lung. *Diagn Cytopathol*. 2006;34(3):224-226.
- Kuroda N, Oonishi K, Ohara M, et al. Invasive micropapillary carcinoma of the colon: an immunohistochemical study. *Med Mol Morphol*. 2007;40(4):226-230.
- Kitagawa H, Nakamura M, Tani T, et al. A pure invasive micropapillary carcinoma of the pancreatic head: long disease-free survival after pancreatoduodenectomy and adjuvant chemotherapy with gemcitabine. *Pancreas*. 2007;35(2):190-192.
- Amin MB, Ro JY, el-Sharkawy T, et al. Micropapillary variant of transitional cell carcinoma of the urinary bladder. Histologic pattern resembling ovarian papillary serous carcinoma. *Am J Surg Pathol*. 1994;18(12):1224-1232.
- Chen L, Fan Y, Lang RG, et al. Breast carcinoma with micropapillary features: clinicopathologic study and long-term follow-up of 100 cases. *Int J Surg Pathol*. 2008;16(2):155-163.
- Li W, Han Y, Wang C, et al. Precise pathologic diagnosis and individualized treatment improve the outcomes of invasive micropapillary carcinoma of the breast: a 12-year prospective clinical study. *Mod Pathol*. 2018;31(6):956-964.
- Guo X, Chen L, Lang R, Fan Y, Zhang X, Fu L. Invasive micropapillary carcinoma of the breast: association of pathologic features with lymph node metastasis. *Am J Clin Pathol*. 2006;126(5):740-746.
- Siriaunkgul S, Tavassoli FA. Invasive micropapillary carcinoma of the breast. *Mod Pathol*. 1993;6(6):660-662.
- Xu X, Bi R, Shui R, et al. Clinicopathological significance of WT1 expression in invasive breast carcinoma with >90% mucinous component. *J Clin Pathol*. 2021;75(12):832-836.
- Wang XX, Liu BB, Wu X, Su D, Zhu Z, Fu L. Loss of leucine zipper putative tumor suppressor 1 (LZTS1) expression contributes to lymph node metastasis of breast invasive micropapillary carcinoma. *Pathol Oncol Res*. 2015;21(4):1021-1026.
- Lv J, Shi Q, Han Y, et al. Spatial transcriptomics reveals gene expression characteristics in invasive micropapillary carcinoma of the breast. *Cell Death Dis*. 2021;12(12):1095.
- Shi Q, Shao K, Jia H, et al. Genomic alterations and evolution of cell clusters in metastatic invasive micropapillary carcinoma of the breast. *Nat Commun*. 2022;13(1):111.
- Faubert B, Solmonson A, DeBerardinis RJ. Metabolic reprogramming and cancer progression. *Science*. 2020;368:6487.
- Griffin JL, Shockcor JP. Metabolic profiles of cancer cells. *Nat Rev Cancer*. 2004;4(7):551-561.
- Schmidt DR, Patel R, Kirsch DG, Lewis CA, Vander Heiden MG, Locasale JW. Metabolomics in cancer research and emerging applications in clinical oncology. *CA Cancer J Clin*. 2021;71(4):333-358.
- Nie M, Yao K, Zhu X, et al. Evolutionary metabolic landscape from preneoplasia to invasive lung adenocarcinoma. *Nat Commun*. 2021;12(1):6479.
- Jarrold J, Davies CC. PRMTs and arginine methylation: Cancer's best-kept secret? *Trends Mol Med*. 2019;25(11):993-1009.
- Guccione E, Richard S. The regulation, functions and clinical relevance of arginine methylation. *Nat Rev Mol Cell Biol*. 2019;20(10):642-657.
- Liu F, Ma F, Wang Y, et al. PKM2 methylation by CARM1 activates aerobic glycolysis to promote tumorigenesis. *Nat Cell Biol*. 2017;19(11):1358-1370.
- Zhong XY, Yuan XM, Xu YY, et al. CARM1 Methylates GAPDH to regulate glucose metabolism and is suppressed in liver cancer. *Cell Rep*. 2018;24(12):3207-3223.
- Liu LM, Sun WZ, Fan XZ, Xu YL, Cheng MB, Zhang Y. Methylation of C/EBPalpha by PRMT1 inhibits its tumor-suppressive function in breast cancer. *Cancer Res*. 2019;79(11):2865-2877.
- He X, Zhu Y, Lin YC, et al. PRMT1-mediated FLT3 arginine methylation promotes maintenance of FLT3-ITD(+) acute myeloid leukemia. *Blood*. 2019;134(6):548-560.
- Xiao N, Nie M, Pang H, et al. Integrated cytokine and metabolite analysis reveals immunometabolic reprogramming in COVID-19 patients with therapeutic implications. *Nat Commun*. 2021;12(1):1618.

28. Cui X, Sawashita J, Dai J, et al. Exercise suppresses mouse systemic AApoAll amyloidosis through enhancement of the p 38 MAPK signaling pathway. *Dis Model Mech*. 2022;15(3):dmm049327.
29. Gao R, Bao J, Yan H, et al. Competition between PAF1 and MLL1/COMPASS confers the opposing function of LEDGF/p75 in HIV latency and proviral reactivation. *Sci Adv*. 2020;6(20):eaaz8411.
30. Lu SC. Regulation of glutathione synthesis. *Mol Asp Med*. 2009;30(1-2):42-59.
31. Di Virgilio F. Purines, purinergic receptors, and cancer. *Cancer Res*. 2012;72(21):5441-5447.
32. Wolfer A, Wittner BS, Irimia D, et al. MYC regulation of a "poor-prognosis" metastatic cancer cell state. *Proc Natl Acad Sci USA*. 2010;107(8):3698-3703.
33. Montaudon E, Nikitorowicz-Buniak J, Sourd L, et al. PLK1 inhibition exhibits strong anti-tumoral activity in CCND1-driven breast cancer metastases with acquired palbociclib resistance. *Nat Commun*. 2020;11(1):4053.
34. Li Z, Wang D, Lu J, et al. Methylation of EZH2 by PRMT1 regulates its stability and promotes breast cancer metastasis. *Cell Death Differ*. 2020;27(12):3226-3242.
35. Choi S, Jung CR, Kim JY, Im DS. PRMT3 inhibits ubiquitination of ribosomal protein S2 and together forms an active enzyme complex. *Biochim Biophys Acta*. 2008;1780(9):1062-1069.
36. Landry-Voyer AM, Bilodeau S, Bergeron D, et al. Human PDCD2L is an export substrate of CRM1 that associates with 40S ribosomal subunit precursors. *Mol Cell Biol*. 2016;36(24):3019-3032.
37. Yao B, Gui T, Zeng X, et al. PRMT1-mediated H4R3me2a recruits SMARCA4 to promote colorectal cancer progression by enhancing EGFR signaling. *Genome Med*. 2021;13(1):58.
38. Beacon TH, Xu W, Davie JR. Genomic landscape of transcriptionally active histone arginine methylation marks, H3R2me2s and H4R3me2a, relative to nucleosome depleted regions. *Gene*. 2020;742:144593.
39. Xu J, Richard S. Cellular pathways influenced by protein arginine methylation: implications for cancer. *Mol Cell*. 2021;81(21):4357-4368.
40. Barski A, Cuddapah S, Cui K, et al. High-resolution profiling of histone methylations in the human genome. *Cell*. 2007;129(4):823-837.
41. Chen X, Cubillos-Ruiz JR. Endoplasmic reticulum stress signals in the tumour and its microenvironment. *Nat Rev Cancer*. 2021;21(2):71-88.
42. Babour A, Bicknell AA, Tourtellotte J, Niwa M. A surveillance pathway monitors the fitness of the endoplasmic reticulum to control its inheritance. *Cell*. 2010;142(2):256-269.
43. Lewis GD, Xing Y, Haque W, et al. Prognosis of lymphotropic invasive micropapillary breast carcinoma analyzed by using data from the National Cancer Database. *Cancer Commun (Lond)*. 2019;39(1):60.
44. Bowen A. Plastic or cast bronchitis? *Am J Dis Child*. 1990;144(10):1075-1076.
45. So MJ, Cheville JC, Katzmann JA, et al. Factors that influence the measurement of prostate cancer DNA ploidy and proliferation in paraffin embedded tissue evaluated by flow cytometry. *Mod Pathol*. 2001;14(9):906-912.
46. Zekioglu O, Erhan Y, Ciris M, Bayramoglu H, Ozdemir N. Invasive micropapillary carcinoma of the breast: high incidence of lymph node metastasis with extranodal extension and its immunohistochemical profile compared with invasive ductal carcinoma. *Histopathology*. 2004;44(1):18-23.
47. Perou CM, Sorlie T, Eisen MB, et al. Molecular portraits of human breast tumours. *Nature*. 2000;406(6797):747-752.
48. Rinschen MM, Ivanisevic J, Giera M, Siuzdak G. Identification of bioactive metabolites using activity metabolomics. *Nat Rev Mol Cell Biol*. 2019;20(6):353-367.
49. Wang Z, Jiang Q, Dong C. Metabolic reprogramming in triple-negative breast cancer. *Cancer Biol Med*. 2020;17(1):44-59.
50. Li W, Tanikawa T, Kryczek I, et al. Aerobic glycolysis controls myeloid-derived suppressor cells and tumor immunity via a specific CEBPB isoform in triple-negative breast cancer. *Cell Metab*. 2018;28(1):87-103 e6.
51. Chen HL, Ding A. Comparison of invasive micropapillary and triple negative invasive ductal carcinoma of the breast. *Breast*. 2015;24(6):723-731.
52. Chalishazar MD, Wait SJ, Huang F, et al. MYC-driven small-cell lung cancer is metabolically distinct and vulnerable to arginine depletion. *Clin Cancer Res*. 2019;25(16):5107-5121.
53. Huang HL, Chen WC, Hsu HP, et al. Argininosuccinate lyase is a potential therapeutic target in breast cancer. *Oncol Rep*. 2015;34(6):3131-3139.
54. Glynn SA, Boersma BJ, Dorsey TH, et al. Increased NOS2 predicts poor survival in estrogen receptor-negative breast cancer patients. *J Clin Invest*. 2010;120(11):3843-3854.
55. Chiang K, Zielinska AE, Shaaban AM, et al. PRMT5 is a critical regulator of breast cancer stem cell function via histone methylation and FOXF1 expression. *Cell Rep*. 2017;21(12):3498-3513.
56. Fulton MD, Cao M, Ho MC, Zhao X, Zheng YG. The macromolecular complexes of histones affect protein arginine methyltransferase activities. *J Biol Chem*. 2021;297(4):101123.
57. Dhar SS, Lee SH, Kan PY, et al. Trans-tail regulation of MLL4-catalyzed H3K4 methylation by H4R3 symmetric dimethylation is mediated by a tandem PHD of MLL4. *Genes Dev*. 2012;26(24):2749-2762.
58. Guenther MG, Levine SS, Boyer LA, Jaenisch R, Young RA. A chromatin landmark and transcription initiation at most promoters in human cells. *Cell*. 2007;130(1):77-88.
59. Sun G, Wang C, Wang S, et al. An H3K4me3 reader, BAP18 as an adaptor of COMPASS-like core subunits co-activates ERalpha action and associates with the sensitivity of antiestrogen in breast cancer. *Nucleic Acids Res*. 2020;48(19):10768-10784.
60. Pokholok DK, Harbison CT, Levine S, et al. Genome-wide map of nucleosome acetylation and methylation in yeast. *Cell*. 2005;122(4):517-527.
61. Cubillos-Ruiz JR, Bettigole SE, Glimcher LH. Tumorigenic and immunosuppressive effects of endoplasmic reticulum stress in cancer. *Cell*. 2017;168(4):692-706.
62. Bartkowiak K, Effenberger KE, Harder S, et al. Discovery of a novel unfolded protein response phenotype of cancer stem/progenitor cells from the bone marrow of breast cancer patients. *J Proteome Res*. 2010;9(6):3158-3168.

SUPPORTING INFORMATION

Additional supporting information can be found online in the Supporting Information section at the end of this article.

How to cite this article: Zhi R, Wu K, Zhang J, et al. PRMT3 regulates the progression of invasive micropapillary carcinoma of the breast. *Cancer Sci*. 2023;114:1912-1928. doi:[10.1111/cas.15724](https://doi.org/10.1111/cas.15724)